

# Vibrational edge modes in intrinsically inhomogeneous doped transition metal oxides

I. Martin, R. J. McQueeney, and A. R. Bishop  
 Los Alamos National Laboratory, Los Alamos, NM 87545

Z. G. Yu  
 SRI International, Menlo Park, CA 94025  
 (December 23, 2021)

By applying an unrestricted Hartree-Fock approximation and a Random Phase approximation to multiband Peierls-Hubbard Hamiltonians, we determine the phonon mode structure in models of transition metal oxides in the presence of intrinsic nanoscale inhomogeneities induced by hole doping. We identify low frequency *local* vibrational modes pinned to the interface between regions of distinct electronic structure and separated in frequency from the band of extended phonons. A major characteristic of these “edge” modes is that their energy is essentially insensitive to the doping level, while their intensity increases with the density of interfaces (and thus doping level). We argue that the presence of such modes is a typical feature of systems with phase separation, including cuprates, nickelates, manganites, and bismuthates. We specifically address the experimental signatures of these modes in lattice inelastic neutron scattering.

Recent advances in experimental techniques provide strong indications that a broad class of electronic materials, commonly referred to as *strongly correlated*, exhibit intrinsically inhomogeneous electronic phases [1–7]. Strong interactions in these materials drive phase separation between regions of distinct electronic structure [8]. However, a competing interaction or electronic kinetic energy can lead to frustration of the global phase separation and to formation of *nanoscale inhomogeneities*, which can take the form of, e.g., stripes [9] or clumps [10]. It has been realized early on that unlike the conventional spin and charge density wave phases, the ordering of intrinsic inhomogeneities is sensitive to thermal and quantum fluctuations [11], as well as static disorder. This makes an unambiguous identification of such phases, and their distinction from the more common density wave instabilities problematic, and therefore requires development of new diagnostics, which are more sensitive to the unique structure of such phases. In this Letter, we propose one such diagnostic tool which relies on detection of localized *edge modes* pinned to the interface between the regions of different electronic structure. While the edge (interface) modes are predicted to appear in every degree of freedom coupled to the inhomogeneity (charge, spin, lattice) [12], here we focus of the *lattice vibrational edge modes* which lend themselves readily to study with inelastic neutron scattering.

We consider two particular classes of transition metal oxides that have attracted significant attention recently – cuprates and nickelates. The former is the material exhibiting high- $T_c$  superconductivity, and the latter is a related compound with Cu replaced by Ni. The Ni-based compounds are typically insulating, with unambiguously demonstrated stripe order [1]. In cuprates, on the other hand, the presence of stripes and their possible influence on superconductivity are subjects of intensive debate. Since it appears that stripes can significantly affect superconductivity [13–15], it is important to establish whether

they are indeed present in the material. Our purpose here is to elucidate typical manifestations of stripe order through a comparative theoretical study of cuprates and nickelates. In particular, we compare these theoretical results to observations of anomalous phonon modes in the cuprates [16–18] and nickelates [19,20]. The results also apply to edge mode signatures in other doped transition metal oxides (and related complex electronic materials), as found in recent experimental studies [19,21–23]; equivalent modes have been predicted and identified in conjugated polymers and quasi-1D (one-dimensional) charge transfer solids [24,25].

We first analyze the signatures of the edge modes in neutron scattering for doped nickelates. To model the  $\text{NiO}_2$  planes, we use a 2D four band extended Peierls-Hubbard Hamiltonian, which includes both electron-electron and electron-phonon interactions [26,27]:

$$H_0 = \sum_{\langle ij \rangle, m, n, \sigma} t_{im,jn} (u_{ij}) (c_{im\sigma}^\dagger c_{jn\sigma} + H.c.) \quad (1)$$

$$+ \sum_{i, m, \sigma} \epsilon_m (u_{ij}) c_{im\sigma}^\dagger c_{im\sigma} + \sum_{\langle ij \rangle} \frac{1}{2} K_{ij} u_{ij}^2 + H_c^{Ni}.$$

Here,  $c_{im\sigma}^\dagger$  creates a hole with spin  $\sigma$  and site  $i$  in orbital  $m$  (there are two nickel orbitals (Ni  $d_{x^2-y^2}$  and  $d_{3z^2-1}$ ) and two oxygen orbitals (O  $p_x$  and  $p_y$ ) included). The bare Ni-O hopping  $t_{im,jn}$  has two values:  $t_{pd}$  between  $d_{x^2-y^2}$  and  $p$  and  $\pm t_{pd}/\sqrt{3}$  between  $d_{3z^2-1}$  and  $p$ . The O site electronic energy is  $\epsilon_p$  and the Ni site energies are  $\epsilon_d$  and  $\epsilon_d + E_z$ , with  $E_z$  the crystal-field splitting on the Ni site. The correlation part of the Hamiltonian is modelled by

$$H_c^{Ni} = \sum_{im} (U + 2J) n_{im\uparrow} n_{im\downarrow} - \sum_{i, m \neq n} 2JS_{im} \cdot S_{in} \quad (2)$$

$$+ \sum_{i, m \neq n, \sigma, \sigma'} (U - J/2) n_{im\sigma} n_{in\sigma'} + \sum_{i, m, n} J c_{im\uparrow}^\dagger c_{im\downarrow}^\dagger c_{in\downarrow} c_{in\uparrow}.$$

Here,  $U$  is the on-site Ni Coulomb repulsion,  $J$  is the Hund coupling that favors a high spin state on Ni sites, and  $\mathbf{S}_{im} = \frac{1}{2} \sum_{\alpha,\beta} c_{im\tau}^\dagger \sigma_{\tau\tau'} c_{im\tau'}$ , with  $\sigma$  the vector of Pauli matrices. The electron-lattice interaction causes modification of the Ni-O hopping strength through the oxygen displacement  $u_{ij}$ :  $t_{im,jn}(u_{ij}) = t_{im,jn}(1 \pm \alpha u_{ij})$ , where  $+$  ( $-$ ) applies if the Ni-O bond shrinks (stretches) for a positive  $u_{ij}$ ; it also affects the Ni on-site energies  $\epsilon_m(u_{ij}) = \epsilon_d + \beta \sum_j (\pm u_{ij})$ , where the sum runs over the four neighboring O ions. The other oxygen modes couple to electron charge more weakly, and are neglected here for simplicity. In our calculations we use the following set of parameters [28,29]:  $\epsilon_p - \epsilon_d = 9$ ,  $U = 4$ ,  $J = 1$ ,  $E_z = 1$ , and  $K = 32/\text{\AA}$  (all in units of  $t_{pd}$ ; we take  $t_{pd} = 1$  eV). The electron-lattice couplings  $\alpha = 3/\text{\AA}$  and  $\beta = 1/\text{\AA}$  were varied to best fit the neutron scattering data. To approximately solve the model, we use unrestricted Hartree-Fock (HF) combined with an inhomogeneous Random Phase Approximation (RPA) for linear lattice fluctuations [26,29] in a supercell of size  $N_x \times N_y$  with periodic boundary conditions. In this model, doped holes tend to segregate into the stripes due to competition between magneto-elastic interaction that favors global electronic phase separation and electronic kinetic energy that favors uniform carrier density. It is worth noting that other competing interactions can produce stripes, clumps and other inhomogeneities [30,31], but the local coupled charge-spin-lattice dynamics governing edge modes on these templates can still be modelled with the above Hamiltonian and RPA analysis.

The output of the calculation is the inhomogeneous HF groundstate and the phonon eigenfrequencies and eigenvectors. From the phonon eigenmodes, we calculate the corresponding neutron scattering cross section, defined as

$$S(\mathbf{k}, \omega) = \int dt e^{-i\omega t} \sum_{ll'} \langle e^{-i\mathbf{k}\mathbf{R}_l(0)} e^{i\mathbf{k}\mathbf{R}_{l'}(t)} \rangle, \quad (3)$$

where  $\mathbf{R}_l(t) = \mathbf{R}_l^0 + \mathbf{d}_l + \mathbf{u}_l(t)$  is the position of the  $l$ -th oxygen atom expressed in terms of the location of the unit cell origin  $\mathbf{R}_l^0$ , position within the unit cell  $\mathbf{d}_l$ , and time-dependent vibrational component  $\mathbf{u}_l(t)$ . For phonon modes with  $\mathbf{u}_l(t)$  oriented along the corresponding metal-oxygen bonds, on the  $\text{O}_x$  sublattice  $\mathbf{d}_l = \frac{a}{2}\hat{x}$  and  $\mathbf{u}_l \equiv x_l\hat{x}$ , and on the  $\text{O}_y$  sublattice  $\mathbf{d}_l = \frac{a}{2}\hat{y}$  and  $\mathbf{u}_l \equiv y_l\hat{y}$ . The scalar displacements can now be expressed in terms of the normal modes  $z_n$  as  $x_l(t) = \sum_n \alpha_{x_l,n} z_n(t)$  and  $y_l(t) = \sum_n \alpha_{y_l,n} z_n(t)$ . Making first order expansion in the oxygen displacements, we obtain

$$S(\mathbf{k}, \omega) = \sum_n \left[ k_x^2 |\alpha_{\mathbf{k},n}^x|^2 + k_y^2 |\alpha_{\mathbf{k},n}^y|^2 + k_x k_y (e^{i(k_x - k_y)a/2} \alpha_{\mathbf{k},n}^x \alpha_{-\mathbf{k},n}^y + c.c.) \right] \times \frac{\hbar}{2m\omega_n} [(1 + n_B)\delta(\omega - \omega_n) + n_B\delta(\omega + \omega_n)]. \quad (4)$$

Here,  $\alpha_{\mathbf{k},n}^x = \sum_l e^{-i\mathbf{k}\mathbf{R}_l^0} \alpha_{x_l,n}$ , and  $n_B = (e^{\omega_n/T} - 1)^{-1}$  is the thermal population of the phonon mode  $n$ . This is a generalization of the usual neutron scattering intensity expression [32] for the case of phonons with a larger real space unit cell. In this paper we plot  $S(\mathbf{k}, \omega)/|\mathbf{k}|^2$  for  $\mathbf{k}$ -directions sampling longitudinal modes, consistent with the common experimental convention.

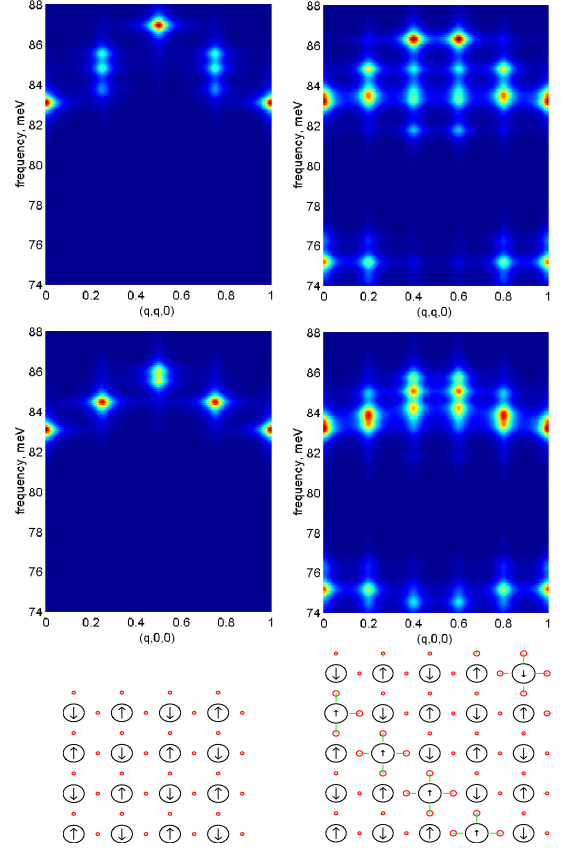


FIG. 1. Neutron scattering spectra and the ground state structures for the undoped (left panels), and hole-doped ( $x = 0.2$ )  $\text{NiO}_2$  planes. The neutron scattering spectra are symmetrized with respect to directions along and across the stripe; in all plots  $q$  runs from 0 to  $2\pi$ . The relative intensity color scheme is defined in Fig. 3. In the lower plots, black circles represent Ni sites and red circles represent O. The radius of a circle is proportional to the corresponding site hole density. Arrows centered on circles show the magnitude and direction of spin. The green lines originating from O sites indicate the magnitude and direction of the equilibrium O displacements due to the formation of a stripe.

The ground state configurations and the corresponding neutron scattering intensities for  $\text{NiO}_2$  planes are shown in Fig. 1. The ground state configuration in the undoped case is a simple antiferromagnet (AF), while, in the doped ( $x = 0.2$ ) case, the holes spatially segregate into a Ni centered stripe along the diagonal of the  $\text{NiO}_2$  plane. The neutron scattering intensities are given in the original Brillouin zone, symmetrized with respect to the orientation of the stripe.

The most striking new feature in the dynamic structure factor that appears upon doping is the creation of the low frequency modes ( $\omega \sim 75$  meV) that split off from the main branch. These low frequency modes have been observed experimentally with inelastic neutron scattering [19,20]. We find that with increasing doping (e.g.,  $x = 0.5$ ) the spectral weight in the new branch increases. However, its energy does not significantly change, nor is there a dependence of the spectrum on the stripe spacing. Intensity to create the local modes is taken from the extended phonon mode branch, with accompanying phase shifts of the extended phonons. There is no simple dispersion that can be associated with the local modes and their wave vectors are related to the characteristic *spatial extent* of the eigenmodes. This is consistent with the doping insensitivity of the phonon “anomaly” observed in neutron scattering experiments for nickelates reported in Ref. [20]. The presence of the phonon edge mode with doping-independent energy is similarly consistent with the doping-insensitivity of the “kink” energy in Angle Resolved Photoemission Spectra (ARPES) reported recently [33] for cuprates (discussed later).

In order to elucidate the structure of these new modes, in Fig. 2 (left panel) we plot a representative mode from this branch. Clearly, this is a mode localized around the stripe edge. For comparison, in the right panel we plot a mode from the high energy branch. Although modified (phase-shifted) due to the presence of a stripe, this mode preserves its original spatially extended structure, characteristic of the undoped case.

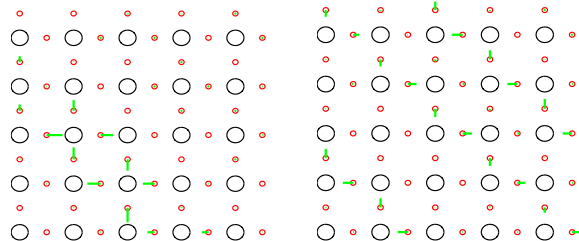


FIG. 2. Representative vibrational eigenmodes for the case of a  $x = 0.2$  doped  $\text{NiO}_2$  plane. Black and red circles represent the equilibrium positions of Ni and O atoms, respectively, and green lines show the magnitude and direction of the O displacement in the mode. On the left, a low frequency mode localized in the vicinity of the stripe ( $E = 75.1$  meV); on the right, an extended phonon with energy  $E = 83.4$  meV.

We now turn to the case of doped  $\text{CuO}_2$  planes for comparison. To this end, we analyze the three-band model analogous to Eqs. (1) and (2), but with only one orbital on the metal site ( $\text{Cu } d_{x^2-y^2}$ ). The electron-electron interactions that we include are the Cu on-site repulsion  $U_d = 8$ , the O on-site repulsion  $U_p = 3$ , and the nearest-neighbor Cu-O repulsion  $U_{pd} = 1$ . The remainder of the parameters are  $\epsilon_p - \epsilon_d = 4$ ,  $K = 32/\text{\AA}$ ,  $\alpha = 4.5/\text{\AA}$  and  $\beta = 1/\text{\AA}$ , with  $t_{pd} = 1.2$  eV [12]. Results of calculations for undoped and doped cuprates are presented in Fig. 3.

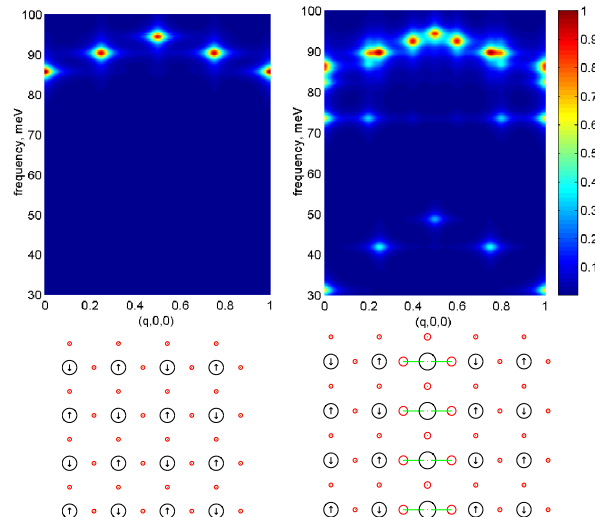


FIG. 3. Neutron scattering spectra and the ground state structures for the undoped (left panels), and hole-doped ( $x = 0.2$ )  $\text{CuO}_2$  planes. The neutron scattering spectra are symmetrized with respect to directions along and across the stripe. In the lower plots, black circles represent Cu sites and red circles represent O. The radius of the circle is proportional to the corresponding site hole density. Arrows centered on circles show the magnitude and direction of spin. The green lines originating from O sites indicate the magnitude and direction of the equilibrium O displacements due to the formation of a stripe.

While generally similar to the  $\text{NiO}_2$ , in the  $\text{CuO}_2$  case doping produces *two* low-frequency branches of localized modes that split off from the band of extended phonon modes. Representative modes from each localized branch are shown in Fig. 4. The lower frequency band centered around  $\sim 40$  meV (left) corresponds to the oxygen displacements along the stripe and the high frequency one at  $\sim 73$  meV to the vibrations perpendicular to the stripe. (The case shown in Fig. 4, right, is a localized asymmetric breathing mode [16,17].) Experimental evidence shows that mode softening of about 15 percent occurs with doping in the cuprates, consistent with the softening predicted here for the *perpendicular* edge mode [16,17]. Recent neutron measurements in twinned and detwinned  $\text{YBa}_2\text{Cu}_3\text{O}_{6+\delta}$  [18] have attempted to resolve the phonon spectrum both parallel and perpendicular to the purported stripe direction [34], but conclusive identification has been hampered by the degeneracy and mixing of many modes near the zone boundary. As yet, there has been no search for the *parallel* edge modes which are predicted here to have a huge softening of  $\sim 60$  percent. However, there are distinct anomalies in the longitudinal phonon spectrum of  $\text{La}_{2-x}\text{Sr}_x\text{CuO}_4$  at 30 meV that have not been studied in detail [17]. Also, it is interesting to mention a possible connection to the “magnetic resonance” mode reported at 41 meV [35]. Note that this low-energy mode (see Fig. 4, left) can only exist for the vertical stripe and hence is absent for the diagonal stripes in the case of  $\text{NiO}_2$  (Fig. 1).

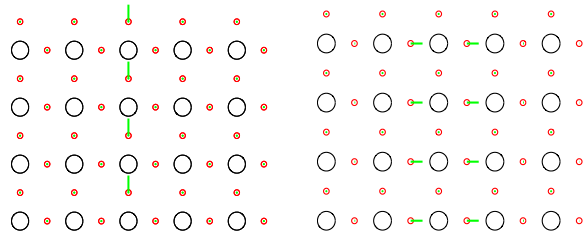


FIG. 4. Localized vibrational eigenmodes for the case of a  $x = 0.2$  doped  $\text{CuO}_2$  plane. The stripe is centered along the middle vertical row of Cu. Unlike the case of diagonal stripes in  $\text{NiO}_2$ , there are two localized branches, one that corresponds to the oxygen vibration parallel to the stripe (low frequency,  $E = 31.2$  meV, on the left), and one that corresponds to the oxygen displacements perpendicular to the stripe (high frequency,  $E = 73.3$  meV, on the right).

Despite the impressive agreement between the energy scales of the predicted and observed modes, it is important to note some deviations from the reported experimental data in terms of the mode intensities and dispersions. We speculate that these discrepancies may be due to the detailed local oxygen environments: either (a) more complex intra-unit cell distortions, i.e. local oxygen polarizations (e.g., from local confinement or pairing effects), which would require more detailed modelling than the constrained O displacements used here, or (b) more complex stripe configurations than the regular linear stripes we have considered above. (Such textured stripe patterns are indeed found in certain models for the origin of stripes [8,31]).

We conclude that the formation of split-off *local* modes, well known in the polaronic physics of conjugated polymers and quasi-1D charge transfer salts [36,24,25], is also expected to be prominently manifested in the case of other doped strongly correlated materials, including nickelates, cuprates, and bismuthates [1–7]. Elsewhere we will report the simultaneous prediction of electron, spin, and lattice edge modes, which should further facilitate the identification of the intrinsically inhomogeneous phases by cross correlating electronic gap modes that occur on eV scale with the localized lattice and spin modes that appear on meV scales. In addition to ARPES and inelastic magnetic and lattice neutron scattering, experimental techniques that could be applied to study the edge modes include infra-red and Raman spectroscopy [24]; resonant Raman scattering would be particularly valuable even for low doping levels [25].

We would like to acknowledge helpful discussions with T. Egami. This work was supported by the U.S. DOE.

---

[1] J. M. Tranquada *et al.*, Phys. Rev. Lett **73**, 1003 (1994).  
[2] J. M. Tranquada *et al.*, Phys. Rev. B **54**, 7489 (1996).  
[3] C. H. Chen, S.-W. Cheong, and A. S. Cooper, Phys. Rev. Lett. **71**, 2461 (1997).  
[4] S.-W. Cheong *et al.*, Phys. Rev. B **49**, 7088 (1994); S.-H. Lee and S.-W. Cheong, Phys. Rev. Lett. **79**, 2514 (1997).

[5] K. Nakajima *et al.*, J. Phys. Soc. Japan **66**, 809 (1997).  
[6] J. M. Tranquada *et al.*, Nature (London) **375**, 561 (1995); J. M. Tranquada *et al.*, Phys. Rev. Lett. **78**, 338 (1997).  
[7] A. P. Ramirez, J. Phys.: Condens. Matter **9**, 8171 (1997).  
[8] E. Dagotto, T. Hotta, and A. Moreo, Physics Reports **344**, 1 (2001); *Intrinsic Multiscale Structure and Dynamics in Complex Oxides*, edited by A. R. Bishop, S. R. Shenoy, and S. Sridar, (World Scientific, Singapore, 2003.)  
[9] J. Zaanen and O. Gunnarsson, Phys. Rev. B **40**, 7391 (1989).  
[10] A. A. Koulakov, M. M. Fogler, and B. I. Shklovskii, Phys. Rev. Lett. **76**, 499 (1996).  
[11] S. A. Kivelson, E. Fradkin, and V. J. Emery, Nature (London) **393**, 550 (1998).  
[12] Z. G. Yu, J. Zang, J. T. Gammel, and A. R. Bishop, Phys. Rev. B **57**, R3241 (1998).  
[13] V. J. Emery, S. A. Kivelson, and O. Zachar, Phys. Rev. B **56**, 6120 (1997).  
[14] I. Martin, G. Ortiz, A. V. Balatsky, A. R. Bishop, Int. J. of Mod. Phys. **14**, 3567 (2000).  
[15] A. Bussman-Holder *et al.*, cond-mat/0012448.  
[16] R. J. McQueeney, *et al.*, Phys. Rev. Lett. **82**, 628 (1999).  
[17] R. J. McQueeney, *et al.*, Phys. Rev. Lett. **87**, 077001 (2001).  
[18] L. Pintschovius, *et al.*, Phys. Rev. Lett. **89**, 037001 (2003); J.-H. Chung, *et al.*, Phys. Rev. B **67**, 014517 (2003); D. Reznik, *et al.*, J. Low Temp. Phys. **131**, 417 (2003).  
[19] J. Tranquada *et al.*, Phys. Rev. Lett **88**, 075505 (2002).  
[20] R. J. McQueeney, J. L. Sarrao, R. Osborn, Phys. Rev. B **60**, 80 (1999).  
[21] M. Braden *et al.*, Physica C **378**, 89 (2002).  
[22] M. d’Astuto *et al.*, Phys. Rev. Lett. **88**, 167002(2002).  
[23] J. Zhang *et al.*, Phys. Rev. Lett. **86**, 3823 (2001).  
[24] J. T. Gammel *et al.*, Phys. Rev. B **45**, 6408 (1992).  
[25] K. Yonemitsu *et al.*, Prog. Theor. Phys. Suppl. **113**, 155 (1993); B. Scott *et al.*, J. Molecular Structure **356**, 207 (1995).  
[26] K. Yonemitsu, A. R. Bishop, and J. Lorenzana, Phys. Rev. B **47**, 12059 (1993).  
[27] Ya-Sha Yi, A. R. Bishop, and H. Röder, J. Phys: Condens. Matter **11**, 3547 (1999).  
[28] J. Zaanen and P. B. Littlewood, Phys. Rev. B **50**, 7222 (1994).  
[29] R. J. McQueeney, A. R. Bishop, Ya-Sha Yi, and Z. G. Yu, J. Phys: Condens. Matter **12**, L317 (2000).  
[30] L. P. Pryadko *et al.*, Phys. Rev. B **60**, 7541 (1999).  
[31] B. P. Stojkovic *et al.*, Phys. Rev. B **62**, 4353 (2000).  
[32] S. W. Lovesy, *Theory of Magnetic Neutron and Photon Scattering* (Oxford, London, 1989).  
[33] A. Lanzara, APS talk (March 2003).  
[34] H. A. Mook, *et al.*, Nature (London) **404**, 729 (2000).  
[35] J. Rossat-Mignod *et al.*, Physica B **192**, 109 (1993).  
[36] K. Fesser, A. R. Bishop, and D. K. Campbell, Phys. Rev. B **27**, 4804 (1983).